

Data Forensics in Diffusion Models: A Systematic Analysis of Membership Privacy

Derui Zhu*

Technical University of Munich

Jens Grossklags

Technical University of Munich

Dingfan Chen*

CISPA Helmholtz Center for Information Security

Mario Fritz

CISPA Helmholtz Center for Information Security

Abstract

In recent years, diffusion models have achieved tremendous success in the field of image generation, becoming the state-of-the-art technology for AI-based image processing applications. Despite the numerous benefits brought by recent advances in diffusion models, there are also concerns about their potential misuse, specifically in terms of privacy breaches and intellectual property infringement. In particular, some of their unique characteristics open up new attack surfaces when considering the real-world deployment of such models. With a thorough investigation of the attack vectors, we develop a systematic analysis of membership inference attacks on diffusion models and propose novel attack methods tailored to each attack scenario specifically relevant to diffusion models. Our approach exploits easily obtainable quantities and is highly effective, achieving near-perfect attack performance (>0.9 AUCROC) in realistic scenarios. Our extensive experiments demonstrate the effectiveness of our method, highlighting the importance of considering privacy and intellectual property risks when using diffusion models in image generation tasks.

1 Introduction

Deep generative modeling has made significant advancements over the past few years, resulting in photo-realistic media generation tools with potential commercial uses for art and design. In particular, the rapid improvement of denoising diffusion models [5, 11, 18, 28, 30–32] has greatly advanced the state-of-the-art in image and video generation tasks, as highlighted in recent studies [5]. Meanwhile, diffusion models are considered the most promising generative framework to date, serving as the foundation for powerful commercial models such as Stable Diffusion [22], Imagen [24], and DALL·E-2 [20].

Despite the remarkable success of recent diffusion models, the widespread use of online APIs and shared pre-trained models raises concerns about their potential risks in various areas. One major concern is the risk of data misuse and violations

of privacy, as sensitive information pertaining to individual identities could be revealed. Additionally, malicious users may attempt to infer the original training data, further exacerbating privacy concerns. An example of such an attack is the membership inference attack (MIA) [27], which seeks to determine if a particular data record was used to train a machine learning model. This is particularly concerning in the context of diffusion models that serve as the backbone for online media editing tools, which are freely accessible to the public.

Another major concern is the potential intellectual property (IP) infringement during the development and deployment of diffusion models. Advanced diffusion models rely heavily on the usage of massive and diverse training data. However, with the commercialization of these models, there is a risk of data being harvested from the internet for model training purposes without proper regard for the IP rights of media creators. Most commonly, it is impractical for model developers to manually review all training samples for IP compliance, making this a relevant issue in real-world application scenarios.

Diffusion models have several distinct features that set them apart from other generative models. First of all, the encoding process in diffusion models is unlearnable and fixed, following a standard procedure that is known to the public. While this eases the training of diffusion models on complex data distributions, it also presents vulnerabilities as attackers can easily and precisely imitate the encoding process, even if the model developer tries to hide it during model deployment. In contrast, attacks on other generative models usually require approximating the encoding process in a lossy manner (e.g., through gradient-based optimization on the model internals [3]). Additionally, the generation process in diffusion models is iterative, resulting in multiple intermediate outputs that may all reveal information about the training samples. Such information can be easily exploited by an attacker to construct dedicated attacks tailored to diffusion models under different deployment scenarios.

In this work, we pioneer the investigation of such risks associated with diffusion models. Specifically, we conduct

* Equal contribution.

the first systematic analysis of MIAs against diffusion models. While previous studies have explored MIAs in the context of both classification models [2, 17, 23, 25, 27, 29, 33] and other generative models [3, 8, 10], we highlight that diffusion models have unique properties and usage patterns that create new attack surface not covered by existing works, and existing methods are not directly applicable to our case. Instead, we thoroughly examine the attack vectors and identify three attack scenarios that are most representative and prevalent in practice, given real-world APIs as reference. Moreover, we design novel attacks tailored to diffusion models based on their unique characteristics, achieving near-perfect (> 0.9 AUCROC) across various practical settings.

Contributions

We make contributions on three levels in this paper, which we categorize as task-level, approach-level, and insight-level.

Task-level: We carry out the first systematic investigation of membership inference attacks on state-of-the-art diffusion models. With a thorough analysis of the potential attack surface, our study reveals the most realistic threat models that reflect actual usage patterns and categorizes attack scenarios into white-box, gray-box, and black-box settings, depending on the information available to the attacker. These categorizations have high practical relevance, reflecting common real-world scenarios while guiding and benchmarking future research in related fields.

Approach-level: We design novel attack strategies for diffusion models, customized to suit various scenarios. Our attacks are based on easily obtainable or estimable quantities and are both straightforward and highly effective, supported by a solid theoretical basis. Moreover, our proposed improvement techniques (e.g., truncation and calibration as discussed in Sections 4.1 and 4.2) significantly enhance attack performance in realistic settings and are highly practical. We anticipate that our proposed method and insights will have broader applications beyond membership inference and be of interest for future tasks involving diffusion models.

Insight-level: We conduct a thorough evaluation of our proposed attack, taking into account various factors such as attack scenarios, data distributions, sample size, target model, and training configurations. We provide a detailed analysis of the key factors that could impact the effectiveness of our attack. We find that our approach is consistently effective across different scenarios. Specifically, having only access to the API, our approach reaches 1.0 AUCROC in CelebA dataset with 5k training samples. When the training sample size increases to 20k, our approach remains effective (attack AUC > 0.85). Lastly, our results suggest an exceptionally high privacy risk of sharing diffusion models as a common practice.

2 Related Work

Generative Models. Generative models aim to simulate the probability distribution of real data by defining a parametric family of densities and finding the optimal parameters. The optimal parameter is typically found by either maximizing the (lower bound of) likelihood of the real data or minimizing the (estimated) divergence between the generated and real data distributions. With the advancement in the expressive power of deep neural networks, recent generative models have achieved significant success in modeling high-dimensional data distributions. Different types of deep generative models have been developed in the literature, with generative adversarial networks (GANs) [7], variational autoencoders (VAEs) [14], and diffusion-based models [11, 28, 30] being the most popular to date. GANs are made up of two modules: the generator and the discriminator, which are trained jointly in a competitive manner. The discriminator is trained to estimate the divergence between the generated and real data distributions, while the generator is optimized to reduce this divergence so as to closely resemble the real data distribution. In contrast, diffusion models follow the variational autoencoding pipeline [14], mapping images to a Gaussian latent space with a pre-defined forward encoding process, then transforming them back to the data space with a denoising decoder. Training is based on a log-likelihood objective.

In this work, we focus on diffusion models, which are the current state-of-the-art deep generative framework [5] and serve as the backbone for various online media generation tools [20, 22, 24]. Additionally, we make connections and comparisons with GANs, which were previously the dominant framework in this field.

Membership Inference Attacks (MIAs). Membership Inference Attack (MIA) was first introduced by Shokri et al. [27]. It focuses on attacking classification models in a black-box setting, where the attacker has access to the victim model’s full response, including confidence scores for all classes, for a given query sample as input. Existing works have developed various approaches in attacking both white-box [17, 21] as well as black-box [23, 25, 27, 29, 33] classification models. Black-box MIAs typically involve training shadow models to extract member and non-member characteristics or utilizing easily accessible information such as losses as the membership indicator. White-box attacks, on the other hand, utilize the target model’s internals (e.g., sample gradients) to construct membership scores. In particular, it has been shown that the sample loss generally can serve as a discriminative signal that tells apart members from non-members [33]. Sablayrolles et al. [23] further showed that black-box attacks can approximate the performance of white-box MIA under certain assumptions on the model parameter distribution. Our approach is built on top of these findings and is specifically tailored for diffusion models by carefully examining their training objectives and potential attack surface during development and deployment.

Recent works have explore such attacks for popular generative models such as GANs [3, 8] and VAEs [10]. Specifically, Hayes et al. [8] observe that disclosing the discriminator in a GAN can result in leaked membership information in a white-box setting and suggested using a shadow model for black-box attacks. Hilprecht et al. [10] proposed using the reconstruction error as a membership score for attacking white-box VAEs and counting generated samples within an ϵ -ball of the query for a black-box membership score. Chen et al. [3] presented a taxonomy of MIAs against GANs and proposed an optimization-based approach for attacks with only generator access and a distance-based approach for the black-box setting with only synthetic samples available.

Our work presents the first systematic analysis of MIAs on diffusion models. Despite similarities in the training objectives with VAEs and comparable generation quality to GANs, diffusion models have distinct properties and unique attack vectors that can be considered and exploited by attackers. We thoroughly examine different attack scenarios specifically relevant to diffusion models and leverage its intrinsic characteristics, such as the pre-defined encoding process and multi-step generation process, to conduct effective attacks. Algorithmically, our approach shares the same high-level concept with existing sample loss-based techniques [3, 23, 33], but differs fundamentally by exploiting the intrinsic properties of diffusion models to make the membership score representative and discriminative, leading to exceptional performance.

3 Background

3.1 Diffusion Models

Formulation. Given observed samples \mathbf{x}_0 from a distribution of interest, the goal of a generative model is to learn to model its true underlying distribution $p(\mathbf{x}_0)$ and generate novel samples from it. Specifically, diffusion models use a forward noising process q , i.e., the “encoding” process, to gradually transform the data distribution into a standard Gaussian $\mathcal{N}(0, \mathbf{I})$. The models then learn to reverse this transformation through a learnable denoising function p_{θ} , i.e., the “decoding” process. Once the denoising function p_{θ} is learned, generating new samples from the data distribution can be achieved by sampling from the standard Gaussian and then iteratively applying the reverse denoising steps $p_{\theta}(\mathbf{x}_{t-1}|\mathbf{x}_t)$. Formally, the forward noising process can be written as follows,

$$q(\mathbf{x}_t|\mathbf{x}_{t-1}) = \mathcal{N}(\mathbf{x}_t; \sqrt{\bar{\alpha}_t}\mathbf{x}_{t-1}, (1 - \alpha_t)\mathbf{I}) \quad (1)$$

where the subscript t is the step index, and α_t is a scaling factor ($0 \leq \alpha_t \leq 1$) controlling the amount of information preserved in each noising step (where a larger α_t means more information is kept). Given a sufficiently large T and an appropriate schedule of α_T , the latent \mathbf{x}_T at the final step forms a standard Gaussian distribution. Meanwhile, the forward pro-

cess defined in Equation 1 allows direct sampling of the noisy latent \mathbf{x}_t at an arbitrary step given the input data \mathbf{x}_0 [11]:

$$q(\mathbf{x}_t|\mathbf{x}_0) = \mathcal{N}(\mathbf{x}_t; \sqrt{\bar{\alpha}_t}\mathbf{x}_0, (1 - \bar{\alpha}_t)\mathbf{I}) \quad (2)$$

$$\mathbf{x}_t = \sqrt{\bar{\alpha}_t}\mathbf{x}_0 + \sqrt{1 - \bar{\alpha}_t}\boldsymbol{\varepsilon} \quad (3)$$

where $\bar{\alpha}_t = \prod_{s=0}^t \alpha_s$ and $\boldsymbol{\varepsilon} \sim \mathcal{N}(0, \mathbf{I})$ denotes a random noise sample. Moreover, the posterior $q(\mathbf{x}_{t-1}|\mathbf{x}_t, \mathbf{x}_0)$ can be computed using Bayes theorem:

$$q(\mathbf{x}_{t-1}|\mathbf{x}_t, \mathbf{x}_0) = \mathcal{N}(\mathbf{x}_{t-1}; \mu_q(\mathbf{x}_t, \mathbf{x}_0), \Sigma_q(t)) \quad (4)$$

$$\mu_q(\mathbf{x}_t, \mathbf{x}_0) = \frac{\sqrt{\bar{\alpha}_t}(1 - \bar{\alpha}_{t-1})\mathbf{x}_t + \sqrt{\bar{\alpha}_{t-1}}(1 - \alpha_t)\mathbf{x}_0}{1 - \bar{\alpha}_t}$$

$$\Sigma_q(t) = \frac{(1 - \alpha_t)(1 - \bar{\alpha}_{t-1})}{1 - \bar{\alpha}_t}\mathbf{I}$$

The joint distribution for the reverse process can be formulated as:

$$p(\mathbf{x}_{0:T}) = p(\mathbf{x}_T) \prod_{t=1}^T p_{\theta}(\mathbf{x}_{t-1}|\mathbf{x}_t) \quad (5)$$

with $p(\mathbf{x}_T) = \mathcal{N}(\mathbf{x}_T; 0, \mathbf{I})$, indicating that the latent distribution at the final step T is a standard Gaussian. The denoising function is modeled as a Gaussian using a neural network as follows:

$$p_{\theta}(\mathbf{x}_{t-1}|\mathbf{x}_t) = \mathcal{N}(\mathbf{x}_{t-1}; \mu_{\theta}(\mathbf{x}_t, t), \Sigma_{\theta}(\mathbf{x}_t, t)) \quad (6)$$

Objective. The diffusion models are trained to maximize the variational lower bound (VLB), i.e., a lower bound of the log-likelihood of the observed data. Formally,

$$\begin{aligned} \log p(\mathbf{x}_0) &\geq \mathbb{E}_{q(\mathbf{x}_1|\mathbf{x}_0)}[\log p_{\theta}(\mathbf{x}_0|\mathbf{x}_1)] - D_{\text{KL}}(q(\mathbf{x}_T|\mathbf{x}_0)||p(\mathbf{x}_T)) \\ &\quad - \sum_{t=2}^T \mathbb{E}_{q(\mathbf{x}_t|\mathbf{x}_0)}[D_{\text{KL}}(q(\mathbf{x}_{t-1}|\mathbf{x}_t, \mathbf{x}_0)||p_{\theta}(\mathbf{x}_{t-1}|\mathbf{x}_t))] \end{aligned}$$

where D_{KL} denotes the KL divergence. The training objective can be equivalently written as minimizing the negative VLB:

$$\boldsymbol{\theta}^* = \arg \min_{\boldsymbol{\theta}} \mathcal{L}_{vlb} = \arg \min_{\boldsymbol{\theta}} \{\mathcal{L}_0 + \mathcal{L}_1 + \dots + \mathcal{L}_T\} \quad (7)$$

$$\mathcal{L}_0 = -\log p_{\theta}(\mathbf{x}_0|\mathbf{x}_1) \quad (8)$$

$$\mathcal{L}_{t-1} = D_{\text{KL}}(q(\mathbf{x}_{t-1}|\mathbf{x}_t, \mathbf{x}_0)||p_{\theta}(\mathbf{x}_{t-1}|\mathbf{x}_t)), \quad 2 \leq t \leq T \quad (9)$$

$$\mathcal{L}_T = D_{\text{KL}}(q(\mathbf{x}_T|\mathbf{x}_0)||p(\mathbf{x}_T)) \quad (10)$$

In practice, \mathcal{L}_0 is computed by discretizing each color component into 256 bins, and evaluating the probability of $p_{\theta}(\mathbf{x}_0|\mathbf{x}_1)$ landing in the correct bin [5, 18]. \mathcal{L}_{t-1} in Equation 9 is computed by sampling from an arbitrary step of the forward noising process (Equation 3) and estimate \mathcal{L}_{t-1} using Equation 4 and 6. Optimizing over the sum in Equation 7 on the training dataset is achieved by randomly sampling t for each image \mathbf{x}_0 in each mini-batch, i.e., approximating \mathcal{L}_{vlb} using the expectation $\mathbb{E}_{t, \mathbf{x}_0, \boldsymbol{\varepsilon}}[\mathcal{L}_t]$.

Parameterization. Recent works develop different ways to parameterize p_{θ} in Equation 6 for solving $\arg \min_{\theta} \mathcal{L}_{t-1}$:

$$\begin{aligned} & \arg \min_{\theta} \mathcal{L}_{t-1} \\ &= \arg \min_{\theta} \frac{1 - \bar{\alpha}_t}{2(1 - \alpha_t)(1 - \bar{\alpha}_{t-1})} \|\mu_{\theta}(\mathbf{x}_t, t) - \mu_{\theta}\|_2^2 \end{aligned} \quad (11)$$

$$= \arg \min_{\theta} \frac{\bar{\alpha}_{t-1}(1 - \alpha_t)}{2(1 - \bar{\alpha}_t)(1 - \bar{\alpha}_{t-1})} \|\hat{\mathbf{x}}_{\theta}(\mathbf{x}_t, t) - \mathbf{x}_0\|_2^2 \quad (12)$$

$$= \arg \min_{\theta} \frac{(1 - \bar{\alpha}_t)(1 - \alpha_t)}{2\alpha_t(1 - \bar{\alpha}_{t-1})} \|\varepsilon_0 - \hat{\varepsilon}_{\theta}(\mathbf{x}_t, t)\|_2^2 \quad (13)$$

$$= \arg \min_{\theta} \frac{(1 - \bar{\alpha}_t)(1 - \alpha_t)}{2\alpha_t(1 - \bar{\alpha}_{t-1})} \|s_{\theta}(\mathbf{x}_t, t) - \nabla \log p(\mathbf{x}_t)\|_2^2 \quad (14)$$

The most obvious option is to let the neural network predict $\mu_{\theta}(\mathbf{x}_t, t)$ directly (Equation 11). Alternatively, the network could predict \mathbf{x}_0 from noisy image \mathbf{x}_t and time index t (Equation 12) [11]. The network could also predict the noise ε_0 that determines \mathbf{x}_t from \mathbf{x}_0 (Equation 13) [11, 24] and the score of the image at an arbitrary noise level, i.e., the gradient of \mathbf{x}_t in data space (Equation 14) [30–32].

Our attack is designed based on the general objective and quantities that all diffusion models rely on, making it easily applicable to existing models and seamlessly adaptable to future advancements. (See Section 4 for more details.)

3.2 Membership Inference

In the standard setting of MIA, the attacker has access to a query set $\mathbb{S} = \{\mathbf{x}^i, m^i\}_{i=1}^N$ with both member (training) and non-member (testing) samples drawn from the same distribution, where m^i is the membership attribute ($m^i = 1$ if \mathbf{x}^i is a member). Unless stated otherwise, the sample index is denoted by the superscript i , and the time step index in a diffusion model is denoted by the subscript t . The task is to determine the membership attribute m^i of each sample \mathbf{x}^i . The attack $\mathcal{A}(\mathbf{x}^i, \mathcal{M}(\theta))$ is a binary classifier that predicts m^i for a given query sample \mathbf{x}^i and a target model \mathcal{M} parametrized by θ , i.e., a diffusion model with model parameter θ . The Bayes optimal attack $\mathcal{A}_{opt}(\mathbf{x}^i, \mathcal{M}(\theta))$ will output 1 if the query sample is more likely to be contained in the training set, based on the real underlying membership probability $P(m^i = 1 | \mathbf{x}^i, \theta)$, which is usually formulated as a non-negative log ratio:

$$\mathcal{A}_{opt}(\mathbf{x}^i, \mathcal{M}(\theta)) = \mathbb{1} \left[\log \frac{P(m^i = 1 | \mathbf{x}^i, \theta)}{P(m^i = 0 | \mathbf{x}^i, \theta)} \geq 0 \right] \quad (15)$$

Our attack is motivated by the recent results showing the dependence of attack success rate on the sample loss [23, 33]. In particular, a large difference in expected loss values between the member and non-member data has been shown to be a sufficient condition for conducting successful attacks [33]. Sablayrolles et al. [23] further prove that the Bayes optimal attack depends only on the sample loss under a

mild posterior assumption of the model parameter, expressed as $\mathcal{P}(\theta | \mathbf{x}^1, \dots, \mathbf{x}^N) \propto e^{-\frac{1}{T} \sum_{i=1}^N m^i \cdot \ell(\theta, \mathbf{x}^i)}$. This corresponds to a Bayesian perspective in which θ is viewed as a random variable that minimizes the empirical risk $\sum_{i=1}^N m^i \cdot \ell(\theta, \mathbf{x}^i)$, and T represents the stochasticity in the model. The optimal attack is then formularized as follows:

$$\mathcal{A}_{opt}(\mathbf{x}^i, \mathcal{M}(\theta)) = \mathbb{1}[\ell(\theta, \mathbf{x}^i) < \tau(\mathbf{x}^i)] \quad (16)$$

where τ denotes a threshold function.

Intuitively, Equation 16 indicates that \mathbf{x}^i is more likely to be a training sample if the target model shows a low loss value for it. Simply applying these results to attacking diffusion models would suggest using the VLB loss \mathcal{L}_{vlb} (Equation 7) as the membership score. However, as demonstrated in Sections 4 and 5, this approach may result in sub-optimal performance or even be infeasible under realistic threat models. Our proposed approach, tailored for each possible threat model, is described in detail in Section 4.

4 General Attack Pipeline

Our attack draws inspiration from previous findings that the sample loss (\mathcal{L}_{vlb} in our case) can serve as a reliable indicator for membership (Section 3.2). However, we uncover several limitations with a straightforward approach and propose modifications tailored to specific threat models. We summarize our threat model in Table 1 and present our proposed improved approach in the upcoming Sections 4.1–4.3.

4.1 White-box setting

Threat Model. We start by investigating the most informed attacker scenario, which is the white-box setting. In this scenario, the attacker has complete access to the trained model parameters θ , as well as the necessary information for model implementation, such as the number of total steps T as well as the (schedule of) scaling factor α_t used in the forward and backward pass. This scenario reflects the common open-source practice of releasing the source code and the pre-trained model checkpoints for public use. These resources, often used as building blocks for image editing tools, are readily available on the internet.

Approach. Existing results suggest that utilizing the sample loss is a viable approach for calculating membership score (see Section 3.2). However, relying solely on \mathcal{L}_{vlb} results in subpar outcomes (see Section 5.2). We conjecture that this is mainly due to the following reasons: First, the randomness in the sampling process during training may cause unequal weight of each term \mathcal{L}_t in the total sum, leading to a deviation from the intended objective \mathcal{L}_{vlb} . More importantly, the large variance in the scale of each term \mathcal{L}_t results in less informative terms dominating the \mathcal{L}_{vlb} sum, leading to a less

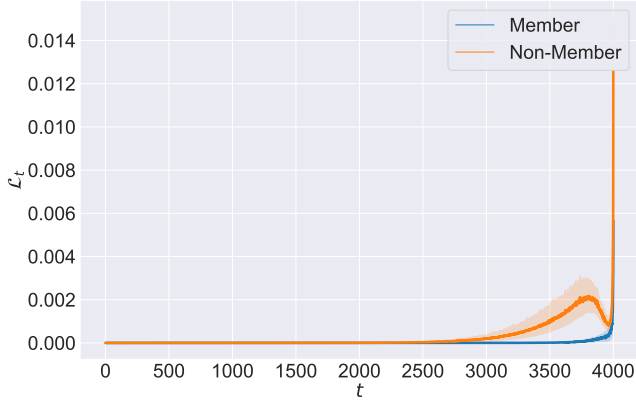


Figure 1: The distribution of \mathcal{L}_t terms for each reverse denoising step of a target diffusion model trained on CelebA with 5k samples.

discriminative outcome for membership inference. As depicted in Figure 1, the terms closer to the noise end (i.e., with a large value of t) have the greatest impact on the VLB loss, but they may be less informative in determining membership. This is because they are close to the Gaussian noise endpoint \mathbf{x}_T and contain limited information about the sample itself \mathbf{x}_0 .

Hence, we propose using the independent terms \mathcal{L}_t that are most discriminative for membership inference instead of \mathcal{L}_{vlb} (the sum of all terms). For this, we focus on terms $0 \leq t \leq T_{\text{trun}}$, where T_{trun} is the point where the loss terms become significantly larger than the previous ones. A simple rule of thumb is to set T_{trun} to approximately $0.75T$, which achieves high effectiveness and is not sensitive to different datasets. In practice, a reasonable choice of T_{trun} can be selected on a small reference set. We also investigate various statistical functions to summarize the loss terms (expressed as a general function f in Equation 17) instead of just the sum as in \mathcal{L}_{vlb} (see Section 5.2). We anticipate that a learnable function f may also be effective, but for simplicity and high attack effectiveness, we use simple statistics such as mean and median. Our attack can be formulated as follows:

$$\mathcal{A}(\mathbf{x}^i, \mathcal{M}(\boldsymbol{\theta})) = \mathbb{1} \left[f \left(\left\{ \mathcal{L}_t(\boldsymbol{\theta}, \mathbf{x}^i) \right\}_{t=0}^{T_{\text{trun}}} \right) < \tau(\mathbf{x}^i) \right] \quad (17)$$

In line with existing results, the attack predicts that a sample belongs to the training set if its overall loss (summarized by f) is lower than a threshold $\tau(\mathbf{x}^i)$. The threshold function can be calibrated to each sample to account for the impact of sample difficulty on membership inference [2, 23].

4.2 Gray-box setting

Threat Model. In this setting, we consider a more realistic scenario where the attacker does not have direct access to the model parameter $\boldsymbol{\theta}$, but can still execute the model. This closely resembles a situation where the model is available to the public through an online API, where the model owner

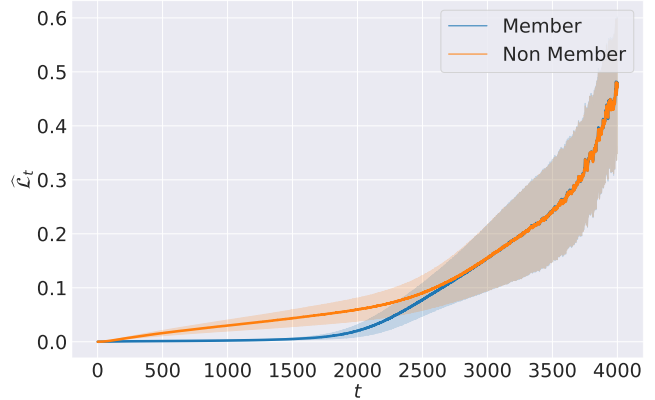


Figure 2: The distribution of $\hat{\mathcal{L}}_t$ terms for each reverse denoising step of a target diffusion model trained on CelebA with 5k samples.

allows others to use the essential functions of the model without disclosing the underlying model. The information that the attacker can exploit may vary depending on the information released through the API. For example, some APIs allow greater control over the generation process, while others do not. Here, we present our attack designed for scenarios that most closely resemble existing real-world APIs and defer the discussion of more relaxed settings to the next subsection.

Approach. Similar to attacking a white-box diffusion model, we still use the sample loss as the membership indicator. However, the attacker does not have direct access to the terms \mathcal{L}_t . Instead, what the attacker can access are the intermediate outputs $\hat{\mathbf{x}}_{\boldsymbol{\theta}}(\mathbf{x}_t, t)$ of the diffusion models applying t denoising steps given the image embedding \mathbf{x}_T . (We consider an image generation model here and discuss the extension to text-to-image models in Section 6.2.) Given a query image \mathbf{x}_0 , the attacker first runs the forward pass to obtain the image embedding \mathbf{x}_T . Note that this requires knowledge or an educated guess about the total number of steps T and the scheduling of the scaling factor α_t . This information is typically displayed on online APIs that allow flexible control of the generation process (e.g., as the "num_inference_steps" and "scheduler" parameters*). The intermediate outputs can be obtained by controlling the number of inference steps t and extracting the corresponding output images displayed on the API. The attack can be formulated as:

$$\mathcal{A}(\mathbf{x}^i, \mathcal{M}(\boldsymbol{\theta})) = \mathbb{1} \left[f \left(\left\{ \hat{\mathcal{L}}_t(\boldsymbol{\theta}, \mathbf{x}^i) \right\}_{t=0}^{T_{\text{trun}}} \right) < \tau(\mathbf{x}^i) \right] \quad (18)$$

with $\hat{\mathcal{L}}_t(\boldsymbol{\theta}, \mathbf{x}^i) = \|\hat{\mathbf{x}}_{\boldsymbol{\theta}}(\mathbf{x}_t^i, t) - \mathbf{x}_0^i\|_2^2$

Compared to the white-box setting, the attack assumption is slightly relaxed in that the attacker needs to estimate the loss terms based on the information typically available on online APIs. Each term of $\hat{\mathcal{L}}_t$ differs from the ground-truth \mathcal{L}_t used in

* Hugging Face Stable Diffusion API: <https://replicate.com/stability-ai/stable-diffusion>

	Model type	Image embedding	Model internals	Hyperparameters T, α_T
white-box (4.1)	✓	✓	□	✓
grey-box (4.2)	✓	✓	■	✓
grey-box extension (6.2)	✓	×	■	✓
black-box specific (4.3)	✓	×	■	×
black-box agnostic (4.3)	×	×	■	×

Table 1: Taxonomy of attack settings. (×: without access; ✓: with access; ■: black-box; □: white-box). "Model type": Whether the underlying model is known to be a diffusion model. "Image embedding": Whether access to the image embedding during generation is available.

the white-box case by a scaling factor (see Equation 12). We deliberately do not use this scaling factor to reduce the impact of the attacker not knowing the exact α_t (this is accessible in some existing APIs but not all of them) and potentially making incorrect guesses in some cases. Additionally, we use the same truncation trick and explore several statistic functions f as in the white-box case to encourage distinguishability in the membership score.

Additionally, we explore the situation where the model owner may reduce the intermediate outputs by subsampling the inference steps, for example, to speed up the generation or limit potential privacy exposure. Formally, the attack in this case can be formulated as follows:

$$\mathcal{A}(\mathbf{x}^i, \mathcal{M}(\boldsymbol{\theta})) = \mathbb{1} \left[f(S) < \tau(\mathbf{x}^i) \right] \quad (19)$$

with $S \subseteq \{\hat{\mathcal{L}}_t(\boldsymbol{\theta}, \mathbf{x}^i)\}_{t=0}^T$

That is, the attacker may only have access to a subset of the intermediate outputs from the reverse denoising steps of the diffusion model. We delve into the truncation techniques specific to this scenario in the experiment section.

4.3 Black-box setting

Threat Model. In this scenario, attackers are limited to passively obtaining generated samples from well-trained generative models, without the ability to affect the generation process. This creates a realistic scenario as there are no set assumptions about the attacker’s abilities. We categorize the situation into two cases based on the attacker’s knowledge of the synthetic data being generated by a diffusion model, referred to as "*known model type*" and "*unknown model type*". In the "*known model type*" case, the attacker recognizes that the accessible synthetic data was produced by a diffusion model and may exploit this information to design targeted attacks. For instance, this may correspond to common situations where the attacker can only collect final outputs from online diffusion model APIs but is not allowed to perform steerable generation, thereby preventing our gray-box attacks discussed in Section 4.2.

Approach. *Model-specific Attack:* Once the attacker knows that the synthetic data set was generated by a diffusion model,

a natural approach would be to train a shadow diffusion model to imitate the target diffusion model by using the synthetic data set as the training set. This enables the attacker to carry out an attack in the same way as in a white-box scenario. This type of attack is referred to as a "*model-specific attack*" to differentiate it from attacks that do not use any information about the generative models. Formally, this can be expressed as:

$$\mathcal{A}(\mathbf{x}^i, \mathcal{M}(\boldsymbol{\theta})) = \mathbb{1} \left[f \left(\left\{ \mathcal{L}_t(\boldsymbol{\theta}^s, \mathbf{x}^i) \right\}_{t=0}^{T_{\text{trun}}} \right) < \tau(\mathbf{x}^i) \right] \quad (20)$$

where $\boldsymbol{\theta}^s$ represents the parameters of the shadow model, which were obtained by training the diffusion model on the synthetic data generated by the target model (parameterized by $\boldsymbol{\theta}$).

Model-agnostic Attack: In the absence of any additional information except for the synthetic sample set, the attacker’s last resort is to use *model-agnostic attacks*. Several options exist in the literature, such as GAN-Leak [3], which uses the Euclidean distance to the nearest neighbor in the synthetic set as a proxy for the sample loss and membership score, and Monte-Carlo [10], which counts the number of generated samples within an ϵ -ball of the query using a carefully designed distance metric. In line with previous work, we use the distance of the query image to its nearest neighbor in the synthetic set as the membership score. Furthermore, we enhance the distance metric by using a pre-trained feature extractor (trained on the large-scale public ImageNet [4] dataset) and further refine the distance calculation by leveraging label information if available. Mathematically,

$$\mathcal{A}(\mathbf{x}^i, \mathcal{M}(\boldsymbol{\theta})) = \mathbb{1} \left[\min_k \left\{ \ell_{dis}(\mathbf{x}^i, \mathbf{s}^k) \right\}_{k=1}^K < \tau(\mathbf{x}^i) \right] \quad (21)$$

with $\mathbf{s}^k \sim p_{\boldsymbol{\theta}}$ representing the samples generated by the target model parameterized by $\boldsymbol{\theta}$. K denotes the total number of synthetic samples, and ℓ_{dis} is the cosine distance in the feature space of a pre-trained ImageNet classifier, where the feature space is determined by the output of the second last layer.

5 Experiment Analysis

In this section, we present the first systematic evaluation of membership inference attacks against state-of-the-art diffusion models. Our comprehensive study encompasses all viable threat models, ranging from the most knowledgeable white-box setting to the most practical black-box one. Importantly, we make key discoveries linking the attack effectiveness to the threat model, data set, model architecture, and training configuration, leading to practical implications for securing the deployment of diffusion models in real-world settings.

5.1 Setup

Datasets. In line with previous research on MIAs against generative models [3, 8], we conduct experiments on bench-

mark image datasets with diverse characteristics.

CelebA [16] is a large-scale face attributes dataset containing 200k RGB images, which are aligned using facial landmarks. To ensure comparability with previous results, we adopt the standard pre-processing procedure when training diffusion models and evaluating attack performance. This involves randomly selecting a maximum of 20k images (corresponding to the more challenging random-split setting in [3]), center-cropping them, and resizing them to a resolution of 64×64 for training the models and evaluating the attacks.

CIFAR-10 [15] is a dataset of 60k RGB images with shape $32 \times 32 \times 3$. Each image is labeled with one of 10 classes, representing the object depicted in the image.

In every setup, we assess the attack effectiveness on a balanced query set \mathbb{S} , i.e., with an equal number of members and non-members.

Target Models. We evaluate two state-of-the-art diffusion models using their official PyTorch implementation: **Improved Diffusion** [18][†] and **Guided Diffusion** [5][‡] (see the Appendix for more details). By default, we set the number of denoising steps T to be 4000 and adopt a standard linear scheduler for α_t . All experiments were conducted on a single NVIDIA A100 GPU.

It is essential to ensure the generation quality of the target models, as attackers are more likely to target models with high utility and practical significance. We present both qualitative and quantitative evaluations of the generation quality in terms of the Fréchet Inception Distance (FID) metric [9] (as shown in Table 6 and Figure 11). A smaller FID value indicates that the generated images are more realistic and closer to the distribution of real data. In particular, our target models generate high-quality output, surpassing the results in previous works [3, 8, 10], demonstrating the high practical value of our study.

Attack Evaluation The proposed membership inference attack is formulated as a binary classification as described in Equations 17–21, with a threshold τ . For simplicity, a sample-independent threshold is used. The attack performance is evaluated by measuring the area under the receiver operating characteristic curve (**AUCROC**), which is obtained by varying τ . The ROC curve is also provided for clear visualization of the attack’s properties, following [2]. Additionally, following [8], the attack **Accuracy** and **F1 Score** are calculated by setting the threshold to the median value of the membership scores over the query set. All these metrics have a value ranging from 0 to 1, with a higher value indicating a more effective attack.

[†] <https://github.com/openai/improved-diffusion>

[‡] <https://github.com/openai/guided-diffusion>

5.2 Evaluation on White-box attack

Effectiveness of Sample Losses as Membership Score.

We initially assess the feasibility of inferring membership with white-box access to a target diffusion model based on the sample loss terms $\{\mathcal{L}_t\}_{t=0}^T$ and/or the VLB loss \mathcal{L}_{vlb} (which represents the sum of all loss terms). As shown in Figure 4, even simply using \mathcal{L}_{vlb} as the membership score achieves promising attack performance. For instance, we obtain 0.62 AUCROC when using \mathcal{L}_{vlb} to attack the target model trained with 20k data samples. The performance improves to 0.68 when we explore various options of the statistical function $f \in \{Sum, Medium, Max, Min\}$ and select the best, which is the "Median" in this setting. The "Average" function is not considered as it is equivalent to "Sum" in terms of discrimination. While we expect that a more complicated design of function f might lead to improved results, we observe that a simple data-independent function works sufficiently well in most cases and stick to such choices throughout our evaluation.

As a reference, previous work reported a maximum AUCROC of 0.61 under comparable conditions (i.e., white-box attack with the same size and type of split in the training set, without using additional reference data) when attacking GANs [3]. Additionally, when the training set size is no larger than 10k, our attack achieves an exceptional performance (AUCROC > 0.9). These results highlight the potential of using sample losses for effective attacks and the significant privacy risk incurred by the common practice of sharing diffusion models in open source.

Performance Gain from Truncation.

To address the instability and indistinguishability caused by large variations in the magnitude of \mathcal{L}_t (as discussed in Section 4.1 and depicted in Figure 1), we improve our attacks by truncating the loss trajectory. This involves excluding the initial denoising steps that have limited relevance to membership but have high values that can easily dominate the statistical function. We present the detailed results in Table 9 (in Appendix) and present the results for the best configuration (f is selected to be "Max" and T_{run} is set to be $0.75T$) in Figure 3(a). As shown in Figure 3(a), our truncation techniques consistently improve the attack performance across various training configurations. In the most challenging setting with a dataset size larger than 15k, the improvement is particularly significant: by around 0.2 AUCROC on CIFAR-10 and 0.25 on CelebA, respectively.

We further show that the performance gain is *not* sensitive to the particular choice of the truncation step T_{run} and training configurations. As can be seen from Table 2 (See Figure 12 for the visualization), a boost in the attack performance can be achieved with a relatively large range of possible values of T_{run} (e.g., when T_{run} is roughly in the range from $0.875T$ to $0.625T$). Moreover, the best value turns out to be consistent across different training settings (i.e., the training set size and

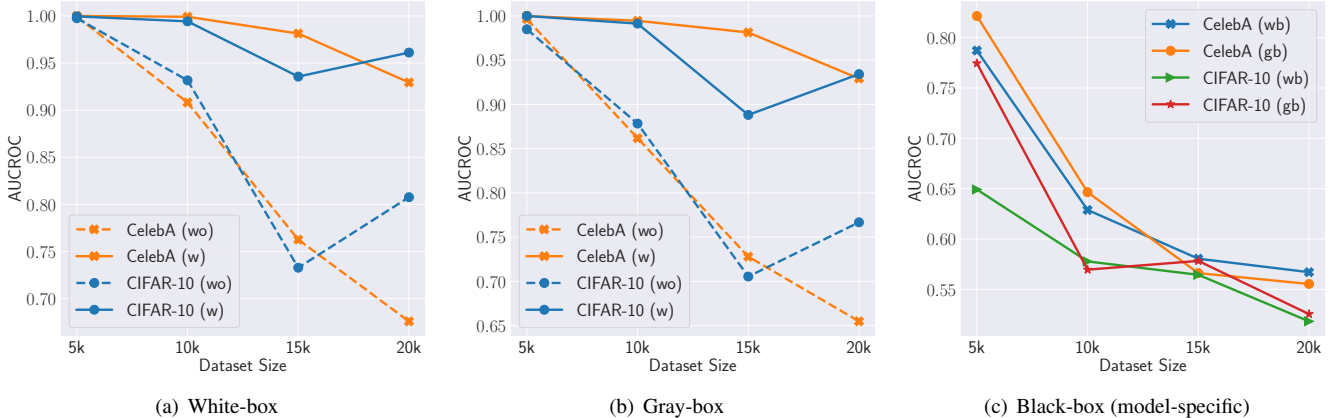


Figure 3: The attack AUCROC across different dataset sizes and attack scenarios. The results obtained with (indicated as "w" and shown as solid lines) and without (indicated as "wo" and shown as dashed lines) applying our truncation techniques are compared. We present the best results for each case where the *Medium* function is used for "wo" truncation and *Max* function is adopted for "w" truncation, the truncation step is always set to be $0.75T$.

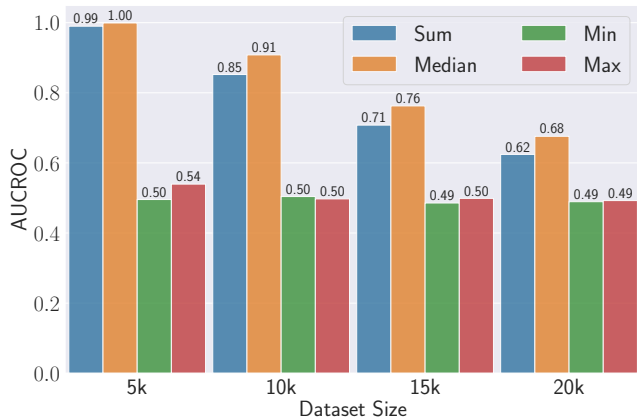


Figure 4: The **white-box** attack AUCROC when applying different statistic function f (*Sum*, *Median*, *Min*, and *Max*) to the *entire loss trajectory* $\{\mathcal{L}_t\}_{t=0}^T$ on CelebA. The "*Sum*" function corresponds to the direct use of \mathcal{L}_{vlb} for MIA.

dataset in our experiments). This suggests a high practical value of our technique such that the attacker may be able to determine the appropriate parameter on any available reference dataset and use such selected parameters for completing the attack. We set by default the statistic function to be a "*Max*" function and T_{trun} to be $0.75T$ for our white-box attack when adopting truncation techniques, which empirically leads to promising performance across various situations.

Effect of Dataset Size. The size of the training dataset is a key determinant of the membership risk associated with machine learning models, as previously noted in the literature [3, 8, 27]. As the number of training samples grows, the model becomes unable to capture the point-wise delta distribution and moves from memorization to generalization. Specifically, previous studies have shown that MIA perfor-

Size	ref	T	$0.975T$	$0.875T$	$0.75T$	$0.625T$	$0.5T$
5k	1.00	0.54	1.00	1.00	1.00	1.00	1.00
10k	0.91	0.50	0.97	1.00	1.00	0.99	0.91
15k	0.76	0.50	0.76	0.97	0.98	0.94	0.76
20k	0.68	0.49	0.65	0.91	0.93	0.86	0.68

Table 2: The **white-box** Attack AUCROC for different truncating steps T_{trun} in CelebA trained with different training data size. The "**ref**" (meaning "reference") column represents the best results that can be achieved without any truncation (but may correspond to different statistic functions). The rest of the results correspond to using a "*Max*" statistic function. The columns, from left to right, represent increasing levels of truncation, excluding the top [0, 100, 500, 1000, 1500, 2000] steps, respectively. The column labeled " T " (in gray) represents "no truncation". The best results (selected to four decimal places) for each configuration are highlighted in bold.

mance tends to be less effective (< 0.6 AUCROC) when the training dataset size exceeds 10k [3, 10].

Consistent with these findings, our results show a tendency of decline in the attack AUCROC as the size of the training dataset grows (refer to Figure 3(a)). However, we observe a consistently high level of attack performance throughout our evaluations, even in cases where previous attacks have typically failed. For example, when the training set size is up to 10k, our attack achieves near-perfect AUCROC on both datasets, and even with a training set size of 20k, our attack remains highly effective (0.93 attack AUCROC for CelebA and 0.96 for CIFAR-10) after applying our truncation techniques.

We additionally present the attack ROC curves in Figure 5 for a more concrete view of the attack performance. Overall, we observe a consistently high level of true positive rate (TPR) even at a generally low level of false positive rate (FPR). We thus conclude that our white-box attack is highly effective, revealing an exceptionally high privacy risk associated with

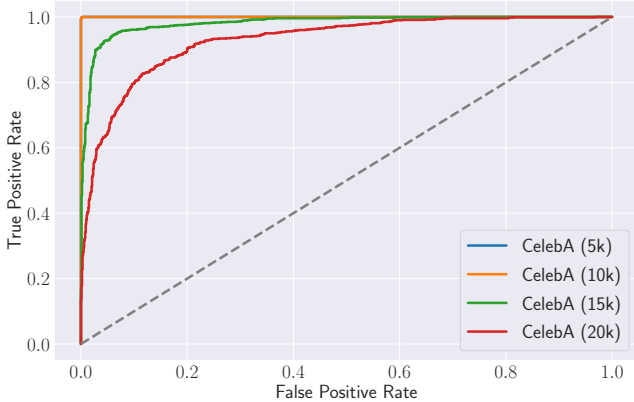


Figure 5: ROC curves of **white-box** (with truncation techniques) attacks on CelebA across different dataset sizes.

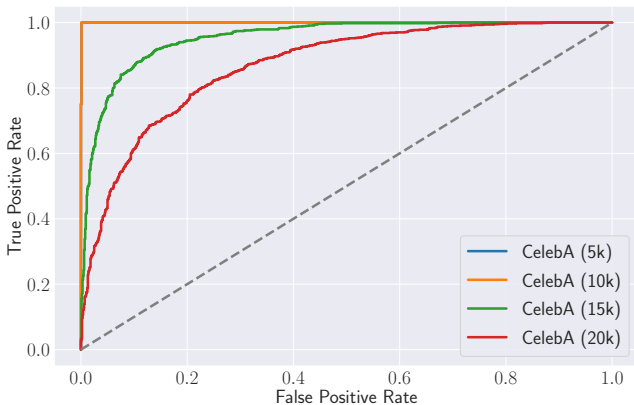


Figure 6: ROC curves of **gray-box** attacks (with truncation techniques) on CelebA across different dataset sizes.

the current open-source practice where the trained diffusion models are accessible to the public.

5.3 Evaluation on Gray-box attack

Estimated Losses as Membership Score. We further consider the real-world scenario where third-party providers, such as Amazon AWS, offer API services to create images using diffusion models. In this scenario, attackers typically have access to the generated images at any inference step of the deployed diffusion model (e.g., by specifying the inference step parameter and obtaining the displayed output), but may not have knowledge of the ground-truth loss terms \mathcal{L}_t (which requires knowing the exact values of α_t). As discussed in Section 4.2, the attack must estimate the loss based on the intermediate output shown on the API. We evaluate the attack performance based on our proposed estimation in Equation 18.

We present our results obtained by using the whole estimated loss trajectories $\{\widehat{\mathcal{L}}_t\}_{t=0}^T$ in Figure 7. As can be seen from the figure, we demonstrate promising performance with an AUCROC of > 0.85 for datasets with up to 10k training

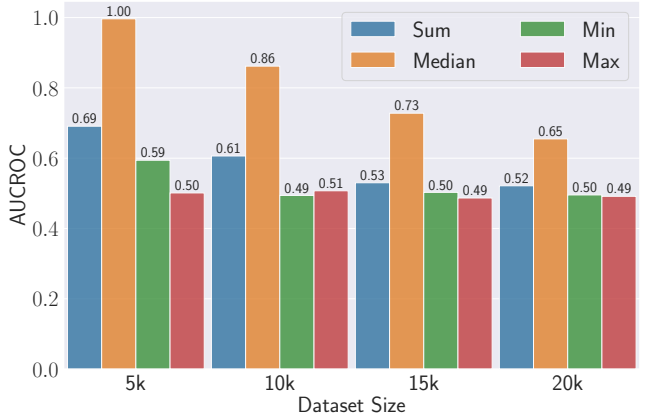


Figure 7: The **gray-box** attack AUCROC when applying different statistic function f (*Sum*, *Median*, *Min*, and *Max*) to the entire loss trajectory estimated based on the intermediate outputs (i.e., $\{\widehat{\mathcal{L}}_t\}_{t=0}^T$) on CelebA.

samples, and an AUCROC value of 0.65 when the dataset size grows to 20k. Despite a slight decrease in comparison to the white-box setting, our gray-box already achieves a reasonable level of performance in its vanilla form, suggesting the potential effectiveness of our formulation. Our results also reveal that "*Medium*" and "*Sum*" statistical functions perform better than the others, with "*Medium*" showing the best performance in most cases across different training configurations. This naturally follows our intuition that using a robust statistic that captures the discriminative factors may be preferable over simply aggregating the available information.

Performance Gain from Truncation. Similar to the case in the white-box setting, not all of the estimated loss terms are informative in distinguishing between members and non-members. Moreover, recall that the generation process in a diffusion model is designed to mimic the reverse denoising process, resulting in noisier outputs in the early denoising stages and thus a larger difference when compared with the clean query sample. By construction, this makes these loss terms corresponding to the earlier denoising steps to have larger magnitudes and to possibly dominate the attack prediction.

Our truncation technique is an effective solution for addressing this issue in the gray-box setting. As demonstrated in Figure 3(b) and detailed in Table 11 (in the Appendix), our truncation technique consistently improves the attack AUCROC by up to 0.25 on CelebA and 0.2 on CIFAR-10, particularly in challenging cases where the training set size is larger than 10k. These cases typically result in less successful attacks with AUCROC less than 0.6 [3], whereas we achieve highly effective attacks with AUCROC around 0.9 throughout our evaluation.

We also studied the impact of various truncation step options on the attack performance. As shown in Figure 8, the

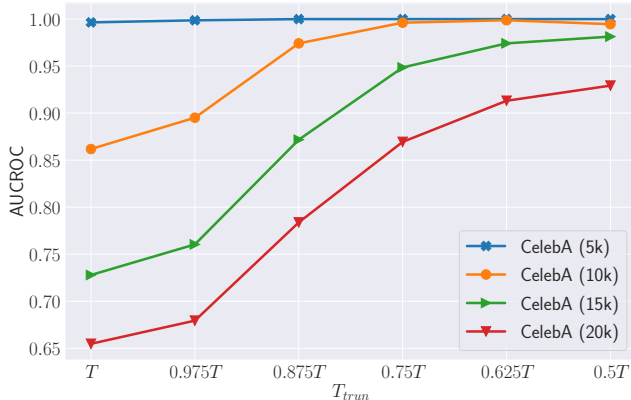


Figure 8: The gray-box Attack AUCROC for different truncating steps T_{trun} across different dataset sizes on CelebA. The statistic function is selected to be "Median".

optimal choice remains largely stable across different training setups (see detailed quantitative results in Table ??). The results indicate that improvements can be achieved with a wide range of reasonable choices. Based on these findings, we set the default truncation step to be $0.5T$ and the "Medium" statistical function as the default for evaluating gray-box attacks with truncation techniques.

Other techniques such as re-weighting and re-scaling the loss terms may also help reduce the significant variation in loss term magnitude and lead to improved results if carefully tuned. However, we believe our truncation technique is advantageous for its simplicity and effectiveness.

Adaptive Defenses. While some of the diffusion APIs expose all the relevant hyperparameters for generation (and attack) and allow controllable synthesis, model owners may decide to withhold certain information to protect commercial interests and preserve privacy, which creates extra challenges for attackers. We study the impact of withholding hyperparameters in diffusion model APIs from an adaptive defense perspective.

We take a more in-depth investigation into the case where the adopted scheduler of α_t is not accessible. While the official implementation supports two scheduler options, we evaluate our attack performance by using a different scheduler than the one used to train the target model. This simulates a worst-case scenario where the attacker guesses the hyperparameter incorrectly. Our results show that our gray-box attacks remain effective even when using a different scheduler (see Table 3), with AUCROC values of 0.91 and 0.65 for datasets of 5k and 20k, respectively. These results suggest that even with a different scheduler, samples can still be mapped to descriptive embeddings in the latent space, revealing information for attack during the reverse generation process. Additionally, as there are only a few options for the scheduler and the forward process is largely the same or highly similar for most diffu-

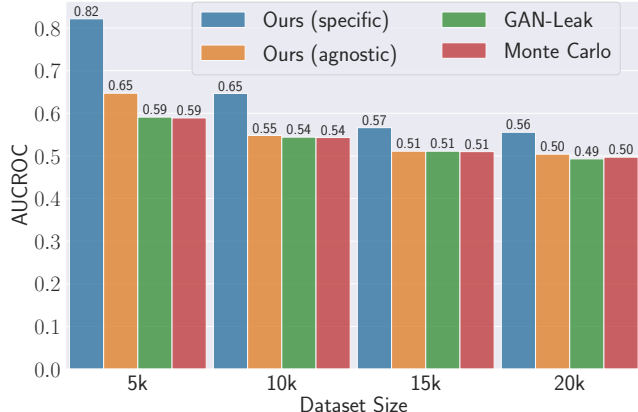


Figure 9: The black-box attack AUCROC on CelebA. We adopt the gray-box attack (with truncation) on the shadow model for our model-specific attack.

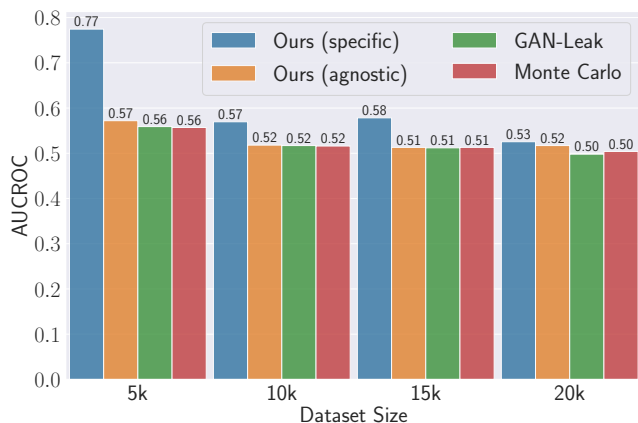


Figure 10: The black-box attack AUCROC on CIFAR-10. We adopt the gray-box attack (with truncation) on the shadow model for our model-specific attack.

sion models, it is likely that the attacker can guess the correct scheduler. This implies that withholding the scheduler may not eliminate the privacy risk.

We also consider the case where the model owner may suppress the intermediate outputs. Table 4 shows the results of suppressing 75% and 50% of the intermediate outputs during the reverse generation process. Our attack is still highly effective in this scenario. Although suppressing the outputs reduces the information leaked to the public and reduces potential risk, we believe that the attacker may still be successful by using proper statistics. This can be seen by examining the distribution of the loss terms, as shown in Figure 2. The attack can exploit a certain range of the discriminative region, and even with suppression, if the attacker can extract a subset of the intermediate outputs, the attack can still perform successful inference.

	5k				20k			
	Medium	Sum	Min	Max	Medium	Sum	Min	Max
w/o	0.62	0.56	0.56	0.49	0.53	0.50	0.49	0.50
w	0.91	0.65	0.56	0.52	0.65	0.54	0.49	0.50

Table 3: The **gray-box** attacks AUCROC on CelebA under wrong guessing of (the scheduler for) α_t with ("w") or without ("wo") applying the truncation technique. The truncation step is set to be the default value $T_{run} = 0.75T$. We highlight the best performance in each configuration in bold.

	75%				50%			
	Medium	Sum	Min	Max	Medium	Sum	Min	Max
w/o	1.00	0.69	0.61	0.51	1.00	0.69	0.57	0.50
w	1.00	0.94	0.61	0.50	1.00	0.94	0.57	0.50

Table 4: The **gray-box** attacks AUCROC on CelebA with 5k training samples when the model owner suppresses the intermediate output (with 75% or 50% suppression ratio). We evaluate both with ("w") and without ("wo") the truncation technique, where the truncation step is always set to $T_{run} = 0.75T$. We highlight the best performance in each configuration in bold.

5.4 Evaluation on Black-box attack

Model-Specific Attack and Cross-model Generalization. The model owner may choose to hide intermediate results when deploying an API, limiting the attacker’s access to only the final synthetic output and limiting control over the generation process. In extreme cases, the attacker may only have access to the final synthetic output without any intermediate results. However, such APIs may still provide clues about the underlying model used [20, 24]. In such cases, training a shadow model as a proxy of the target and conducting the attack on the shadow model would be a good strategy.

With a proxy model in hand, the attacker can apply either white-box or gray-box attack techniques discussed previously. We present results using the default settings for both white-box and gray-box attacks with truncation in Figure 3(c). The attack performance decreases as the dataset size increases, but reasonable levels of AUCROC values above 0.6 are still obtained for datasets smaller than 10k. The performance of the gray-box and white-box attacks is generally comparable. By default, we use the gray-box attack with truncation for further evaluation due to its overall stability.

We take a step further into the investigation of the cross-architecture generalization of our model-specific black-box attack. Specifically, we study the scenario where the shadow model has a different architecture and may adopt a different setup of the key hyperparameters than the target model. As seen in Table 5, there is a slight decrease in attack AUCROC (0.77) compared to when the shadow model and target model have the same architecture (AUCROC 0.82). Furthermore, changing the key hyperparameter (the denoising step in our case) also results in a slight decrease in AUCROC from 0.77 to 0.73, but the change is not substantial. This aligns with

previous research findings, as changing the architecture can cause the shadow model to be less similar to the target model.

However, the difference in architecture may have less impact on attacks against generative models compared to classification models. In the black-box scenario, membership information in generative models is completely contained in the generated distribution, which can still be captured by a shadow model with a different architecture. In contrast, for classification models, membership information is mainly represented by their specific responses to each query, which can vary greatly between models with different architecture. Therefore, attacks based on shadow models remain relatively effective in cross-architecture scenarios for generative models, unlike MIAs against classification models that tend to become less effective [8, 27].

Diffusion Steps	AUCROC	Accuracy	F1-Score
2000	0.73	0.68	0.68
4000	0.77	0.69	0.69
6000	0.76	0.68	0.68

Table 5: The **black-box** attack performance when attacking a *guided diffusion model* with an *improved diffusion model* as the shadow model. Different settings of the diffusion steps are considered when training the shadow model. The experiments were carried out on the CelebA dataset with 5k training samples.

Model-based vs. Model-agnostic For the least informed attack scenario, attackers would have to rely on a model-agnostic method, i.e., they cannot use any extra knowledge of the target model except blindly collecting generated samples from it. In this case, we build upon existing methods that calculate the distance between the query sample and generated samples (closer distance indicates higher membership probability). We improve upon these methods by enhancing the distance metrics, i.e., we use a pre-trained ImageNet classifier as a feature extractor and compute the cosine distance between features as the metrics. Our modification leverages the rich semantic information from the pre-trained feature extractor to improve the discriminative power of the resulting membership score. The comparisons to existing methods are shown in Figures 9 and 10. As shown, our model-agnostic attack performs slightly better than existing methods, while our model-specific attack greatly improves by leveraging slightly more information that is always freely available even in a black-box setting.

5.5 MIA Comparison between Diffusion Models and GANs

Our results presented in previous sections suggest that diffusion models may be generally more vulnerable to MIAs in comparison to other popular generative models such as GANs

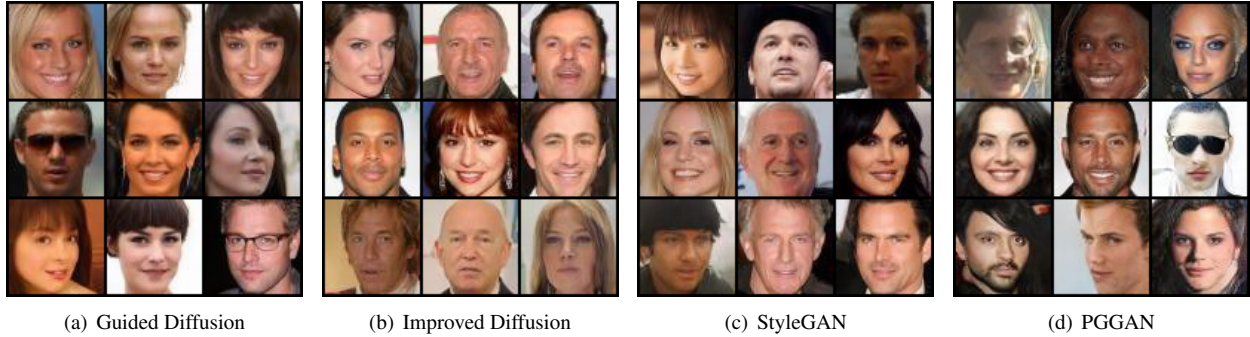


Figure 11: The synthetic images sampled from Guided Diffusion, Improved Diffusion, StyleGAN and PGGAN trained on Celeba with 5k samples, respectively.

under various attack scenarios. In this section, we closely examine their behavior under MIAs in a similar setting. We train and evaluate both diffusion and GAN models on the same sample set using the same attack methods. We consider the most widely used state-of-the-art models or the previous state-of-the-art at their release time. These include two GAN models, namely the StyleGAN [13] and progressive GAN (PGGAN) [12], and the "Guided" and "Improved" diffusion models. The results in Table 6 show that diffusion models have higher attack AUCROC compared to GAN models, with PGGAN having 0.56 and Improved Diffusion having 0.62. This confirms that diffusion models are indeed more vulnerable to MIA attacks than GAN models, even when considering only model-agnostic attacks, not to mention the exceptionally high privacy risk when our dedicated approaches are applied.

	Guided	Improved	StyleGAN	PGGAN
FID	22.46	24.78	25.89	55.28
GAN-Leak	0.59	0.62	0.51	0.57
MC	0.59	0.61	0.51	0.56

Table 6: The attack AUCROC and the FID of various generative models trained on the CelebA dataset using 5k training samples. The FID was calculated based on 40k generated images from each generative model.

6 Discussion

In this section, we highlight several key insights and their practical implications, as well as discuss possible concerns regarding our attack formulation.

6.1 Privacy Risks of Diffusion Models

Our results in Section 5 show that MIAs have a notably higher attack success rate when targeting diffusion models compared to other popular generation models like GANs across various attack scenarios. This can be attributed to the objective used by diffusion models. The objective, which is to maximize the log-likelihood lower bound on all training samples, can result

in a loss landscape that locally minimizes the loss around each training sample, potentially leading to a Dirac delta distribution if not properly regularized. This inevitably leaves clues for attackers to successfully conduct their attacks. In contrast, the adversarial objective used in GANs indirectly guides the generator to produce samples that resemble the training data, while also preventing exact memorization through adversarial updates. These indicate that diffusion models may intrinsically pose a higher privacy risk and should be used with caution in real-world applications, especially considering their widespread use as a standard media generation tool.

Additionally, it is relatively easy to reduce privacy risk for other generative models by only releasing the functional part (e.g. the generator) and keeping the unnecessary part (e.g. the encoder in VAEs or the discriminator in GANs) private [3]. However, this is normally not the case for diffusion models, since the unnecessary part of diffusion models (the forward process) is fixed, unlearned, identical or highly similar across models and settings, making it easy for the attacker to guess and mimic the real process and thus incurs much higher potential risks in the deployment scenarios.

6.2 Conditional Generation

While this work focuses on image generation models, exploring possible extensions to popular conditional generation tools, such as text-to-image [20, 22, 24] and image-to-image [5] models, is an interesting direction. In the white-box case where the model internals are accessible, our attack can be easily applied to the image generation part if only the image embedding determines the generation process. However, if the generation part requires both image embedding and additional information, mapping the image embedding to the space of the conditioning information, such as text embedding, may be necessary. This can be achieved using pre-trained models, such as image captioning to generate descriptive text from query images or the CLIP model [19] to match the image embedding with the text embedding in a semantic preserving way. The same situation applies to the gray-box setting,

which typically requires such extra mappings. Recent works have shown promising results using pre-trained models for deepfake detection in diffusion models [26], and we expect positive outcomes in the task of membership inference. However, more in-depth investigation is needed and is left for future work as it requires dedicated effort to reverse engineer the appropriate mapping given the target conditional generation method’s implementation information and is orthogonal to our contributions in this work.

6.3 Potential Defenses

As presented in Section 5.4, limiting the information available to attackers is generally effective in protecting against such attacks. A slight decrease in attack performance can occur when the model developer hides important parameters, causing the attacker to make incorrect guesses, while a larger degradation happens when the model owner further prevents controllable generation (comparing gray-box to black-box model-specific attacks) and even obscures the sources of synthetic samples (comparing model-specific to model-agnostic attacks). However, these measures can come at the cost of a degraded user experience and may not be a sustainable solution.

Providing rigorous privacy guarantees is another option for the defense. Differential privacy (DP) [6] is a widely used technique that ensures protection against privacy attacks. To prevent privacy leakage from machine learning models, DP incorporates adding random noise to the gradients during training to reduce the impact of each individual sample on the model parameter and thus hide the presence of the data in the training set [1]. However, DP training inevitably hampers the model utility and increases the computational cost during training. While notable recent progress has been achieved in developing DP generative models, these advancements are largely limited to simple datasets and do not offer a practical solution for the complex datasets considered in this work.

7 Conclusion

In this work, we present the first systematic analysis of membership inference attacks against diffusion models. Our work presents for the first time the key attack vectors that are particularly relevant for real-world deployment scenarios of diffusion models. Moreover, we propose our novel attack approaches tailored to each attack scenario, which exploit easily obtainable information while achieving promising performance across a wide range of setups. Our results highlight the high potential privacy risk associated with diffusion models with which we aim to motivate further efforts into related topics.

References

- [1] Martin Abadi, Andy Chu, Ian Goodfellow, H Brendan McMahan, Ilya Mironov, Kunal Talwar, and Li Zhang. Deep learning with differential privacy. In *Proceedings of the 2016 ACM SIGSAC Conference on Computer and Communications Security (CCS)*, 2016.
- [2] Nicholas Carlini, Steve Chien, Milad Nasr, Shuang Song, Andreas Terzis, and Florian Tramèr. Membership inference attacks from first principles. In *2022 IEEE Symposium on Security and Privacy (SP)*. IEEE, 2022.
- [3] Dingfan Chen, Ning Yu, Yang Zhang, and Mario Fritz. Gan-leaks: A taxonomy of membership inference attacks against generative models. In *Proceedings of the 2020 ACM SIGSAC Conference on Computer and Communications Security (CCS)*, 2020.
- [4] Jia Deng, Wei Dong, Richard Socher, Li-Jia Li, Kai Li, and Li Fei-Fei. Imagenet: A large-scale hierarchical image database. In *2009 IEEE Conference on Computer Vision and Pattern Recognition (CVPR)*. IEEE, 2009.
- [5] Prafulla Dhariwal and Alexander Nichol. Diffusion models beat GANs on image synthesis. *Advances in Neural Information Processing Systems (NeurIPS)*, 34, 2021.
- [6] Cynthia Dwork, Aaron Roth, et al. The algorithmic foundations of differential privacy. *Foundations and Trends® in Theoretical Computer Science*, 2014.
- [7] Ian Goodfellow, Jean Pouget-Abadie, Mehdi Mirza, Bing Xu, David Warde-Farley, Sherjil Ozair, Aaron Courville, and Yoshua Bengio. Generative adversarial nets. In *Advances in Neural Information Processing Systems (NeurIPS)*, volume 27, 2014.
- [8] Jamie Hayes, Luca Melis, George Danezis, and Emiliano De Cristofaro. Logan: Membership inference attacks against generative models. *Proceedings on Privacy Enhancing Technologies*, 2019(1), 2019.
- [9] Martin Heusel, Hubert Ramsauer, Thomas Unterthiner, Bernhard Nessler, and Sepp Hochreiter. GANs trained by a two time-scale update rule converge to a local nash equilibrium. *Advances in Neural Information Processing Systems (NeurIPS)*, 30, 2017.
- [10] Benjamin Hilprecht, Martin Härterich, and Daniel Bernau. Monte Carlo and reconstruction membership inference attacks against generative models. *Proceedings on Privacy Enhancing Technologies*, 2019(4), 2019.
- [11] Jonathan Ho, Ajay Jain, and Pieter Abbeel. Denoising diffusion probabilistic models. *Advances in Neural Information Processing Systems (NeurIPS)*, 33, 2020.

- [12] Tero Karras, Timo Aila, Samuli Laine, and Jaakko Lehtinen. Progressive growing of GANs for improved quality, stability, and variation. In *International Conference on Learning Representations (ICLR)*.
- [13] Tero Karras, Samuli Laine, and Timo Aila. A style-based generator architecture for generative adversarial networks. In *Proceedings of the IEEE/CVF Conference on Computer Vision and Pattern Recognition (CVPR)*, 2019.
- [14] Diederik P. Kingma and Max Welling. Auto-encoding variational Bayes. In *International Conference on Learning Representations (ICLR)*, 2014.
- [15] Alex Krizhevsky. *Learning multiple layers of features from tiny images*. M.Sc. Thesis, University of Toronto, 2009.
- [16] Ziwei Liu, Ping Luo, Xiaogang Wang, and Xiaoou Tang. Deep learning face attributes in the wild. In *Proceedings of International Conference on Computer Vision*, December 2015.
- [17] Milad Nasr, Reza Shokri, and Amir Houmansadr. Comprehensive privacy analysis of deep learning: Passive and active white-box inference attacks against centralized and federated learning. In *2019 IEEE Symposium on Security and Privacy (SP)*. IEEE, 2019.
- [18] Alexander Quinn Nichol and Prafulla Dhariwal. Improved denoising diffusion probabilistic models. In *International Conference on Machine Learning (ICML)*. PMLR, 2021.
- [19] Alec Radford, Jong Wook Kim, Chris Hallacy, Aditya Ramesh, Gabriel Goh, Sandhini Agarwal, Girish Sastry, Amanda Askell, Pamela Mishkin, Jack Clark, et al. Learning transferable visual models from natural language supervision. In *International Conference on Machine Learning (ICML)*. PMLR, 2021.
- [20] Aditya Ramesh, Prafulla Dhariwal, Alex Nichol, Casey Chu, and Mark Chen. Hierarchical text-conditional image generation with CLIP latents. *arXiv preprint arXiv:2204.06125*, 2022.
- [21] Shahbaz Rezaei and Xin Liu. Towards the infeasibility of membership inference on deep models. *arXiv preprint arXiv:2005.13702*, 2020.
- [22] Robin Rombach, Andreas Blattmann, Dominik Lorenz, Patrick Esser, and Björn Ommer. High-resolution image synthesis with latent diffusion models. In *Proceedings of the IEEE/CVF Conference on Computer Vision and Pattern Recognition (CVPR)*, 2022.
- [23] Alexandre Sablayrolles, Matthijs Douze, Yann Ollivier, Cordelia Schmid, and Hervé Jégou. White-box vs black-box: Bayes optimal strategies for membership inference. In *International Conference on Machine Learning (ICML)*. PMLR, 2019.
- [24] Chitwan Saharia, William Chan, Saurabh Saxena, Lala Li, Jay Whang, Emily Denton, Seyed Kamyar Seyed Ghasemipour, Burcu Karagol Ayan, S. Sara Mahdavi, Rapha Gontijo Lopes, et al. Photorealistic text-to-image diffusion models with deep language understanding. *arXiv preprint arXiv:2205.11487*, 2022.
- [25] Ahmed Salem, Yang Zhang, Mathias Humbert, Mario Fritz, and Michael Backes. ML-Leaks: Model and data independent membership inference attacks and defenses on machine learning models. In *Annual Network and Distributed System Security Symposium (NDSS)*, 2019.
- [26] Zeyang Sha, Zheng Li, Ning Yu, and Yang Zhang. De-fake: Detection and attribution of fake images generated by text-to-image diffusion models. *arXiv preprint arXiv:2210.06998*, 2022.
- [27] Reza Shokri, Marco Stronati, Congzheng Song, and Vitaly Shmatikov. Membership inference attacks against machine learning models. In *2017 IEEE Symposium on Security and Privacy (SP)*, pages 3–18. IEEE, 2017.
- [28] Jascha Sohl-Dickstein, Eric Weiss, Niru Maheswaranathan, and Surya Ganguli. Deep unsupervised learning using nonequilibrium thermodynamics. In *International Conference on Machine Learning (ICML)*. PMLR, 2015.
- [29] Liwei Song and Prateek Mittal. Systematic evaluation of privacy risks of machine learning models. In *USENIX Security Symposium*, 2021.
- [30] Yang Song and Stefano Ermon. Generative modeling by estimating gradients of the data distribution. *Advances in Neural Information Processing Systems (NeurIPS)*, 32, 2019.
- [31] Yang Song and Stefano Ermon. Improved techniques for training score-based generative models. *Advances in Neural Information Processing Systems (NeurIPS)*, 33, 2020.
- [32] Yang Song, Jascha Sohl-Dickstein, Diederik P. Kingma, Abhishek Kumar, Stefano Ermon, and Ben Poole. Score-based generative modeling through stochastic differential equations. In *International Conference on Learning Representations (ICLR)*.
- [33] Samuel Yeom, Irene Giacomelli, Matt Fredrikson, and Somesh Jha. Privacy risk in machine learning: Analyzing the connection to overfitting. In *IEEE 31st Computer Security Foundations Symposium (CSF)*. IEEE, 2018.

A Experiment Configuration

We demonstrate the details of our experimental setup in this section. Table 7 shows the hyperparameters that we applied in training guided diffusion and improved diffusion models. We trained the guided diffusion models with the default setting on CelebA and CIFAR-10 with 5k, 10k, 15k and 20k data samples, respectively. For styleGAN and PGGAN, we trained the models on 5000 samples randomly drawn from the CelebA and CIFAR-10 datasets. We use the officially released implementation to train the models with the default parameters setting.

Hyperparameters	Guided Diffusion	Improved Diffusion
channels	128	128
residual block	3	3
learn sigma	True	True
noise scheduler	linear	linear
batch size	256	256
learning rate	1e-3	1e-3
diffusion steps	4000	2000;4000;6000
dropout	0.3	0.3

Table 7: The Training Hyperparameters for Guided Diffusion and Improved Diffusion models.

B Additional Results

B.1 White-box Setting

We present the investigation of various statistic functions f on the loss trajectory on CIFAR-10 dataset in Table 8. The results confirm the consistency with findings from experiments on the CelebA dataset.

Size	Truncation	Min	Max	Medium	Sum
5000	without	0.51	0.54	0.99	0.99
	with	0.54	0.64	0.99	0.99
10000	without	0.50	0.50	0.91	0.85
	with	0.54	0.66	0.99	0.99
15000	without	0.49	0.50	0.76	0.71
	with	0.58	0.60	0.99	0.99
20000	without	0.49	0.68	0.49	0.62
	with	0.49	0.52	0.93	0.84

Table 8: The **white-box** attack AUCROC when applying different statistic function f (*Min*, *Max*, *Medium*, and *Sum*) to the loss trajectory $\{\mathcal{L}_t\}_{t=0}^T$ with and without truncations. The experiments were conducted on the CIFAR-10 dataset with various training set sizes, as indicated in the first column. For the cases where the truncation technique is applied, we set the truncation step to be the default value with $T_{trun} = 0.75T$.

Additionally, we examine the potential factors that may

impact the vulnerability of target diffusion models to MIA, such as truncating loss trajectory, statistical functions, training set size, etc. Our extended experiments on the CelebA dataset cover various training configurations, and the results are displayed in Table 9.

(a) CelebA (5k)						
f	T	$0.975T$	$0.875T$	$0.75T$	$0.625T$	$0.5T$
Median	1.00	1.00	0.99	0.94	0.77	0.56
Sum	0.99	1.00	1.00	1.00	1.00	0.97
Min	0.50	0.50	0.50	0.50	0.50	0.50
Max	0.54	1.00	1.00	1.00	1.00	1.00

(b) CelebA (10k)						
f	T	$0.975T$	$0.875T$	$0.75T$	$0.625T$	$0.5T$
Median	0.91	0.89	0.78	0.62	0.52	0.50
Sum	0.85	1.00	1.00	0.99	0.91	0.71
Min	0.50	0.50	0.50	0.50	0.50	0.50
Max	0.50	0.97	1.00	1.00	0.99	0.91

(c) CelebA (15k)						
f	T	$0.975T$	$0.875T$	$0.75T$	$0.625T$	$0.5T$
Median	0.76	0.74	0.64	0.55	0.51	0.50
Sum	0.71	0.93	0.97	0.92	0.78	0.60
Min	0.49	0.49	0.49	0.49	0.49	0.49
Max	0.50	0.76	0.97	0.98	0.94	0.76

(d) CelebA (20k)						
f	T	$0.975T$	$0.875T$	$0.75T$	$0.625T$	$0.5T$
Median	0.68	0.65	0.58	0.52	0.50	0.49
Sum	0.62	0.84	0.90	0.84	0.70	0.56
Min	0.49	0.49	0.49	0.49	0.49	0.49
Max	0.49	0.65	0.91	0.93	0.86	0.68

Table 9: The **white-box** attacks AUCROC with different statistic function f and truncation steps T_{trun} (shown in each column) on CelebA across various training set sizes (shown in the title of each sub-table). The first column T corresponds to "no truncation".

We present the quantitative results in Table 10, which is supplementary to Figure 3(a) in the main paper.

Truncation	CelebA				CIFAR-10			
	5k	10k	15k	20k	5k	10k	15k	20k
w/o	1.00	0.91	0.76	0.68	1.00	0.93	0.73	0.81
w	1.00	1.00	0.98	0.93	1.00	0.99	0.94	0.96

Table 10: The **white-box** attack AUCROC across different training set sizes. Without ("w/o") truncation, the statistic function is selected to be "*Median*", while it is set to be "*Max*" with ("w") truncation. The truncation step is set to be $T_{trun} = 0.75T$.

We visualize the results of our white-box attack across various settings of the truncation steps on the CelebA dataset across various training configurations. We present the results in Figure 12. This is supplementary to the results in Table 2

in the main paper.

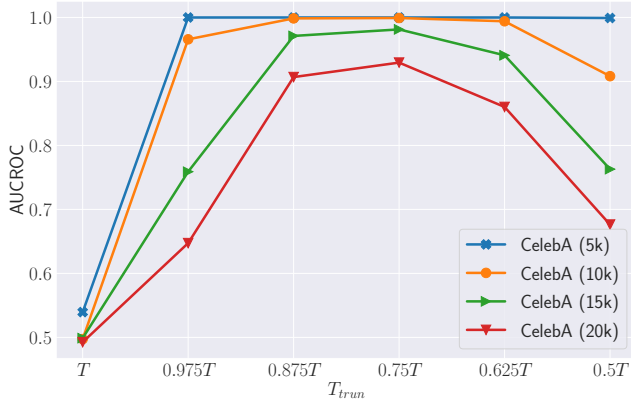


Figure 12: The **white-box** Attack AUCROC for different truncating steps T_{trun} across different dataset sizes on CelebA. The statistic function is selected to be "Max".

B.2 Gray-box Setting

(a) CelebA (5k)

f	T	$0.975T$	$0.875T$	$0.75T$	$0.625T$	$0.5T$
Medium	1.00	1.00	1.00	1.00	1.00	1.00
Sum	0.69	0.71	0.80	0.94	1.00	1.00
Min	0.59	0.56	0.55	0.55	0.58	0.55
Max	0.50	0.50	0.50	0.54	0.66	1.00

(b) CelebA (10k)

f	T	$0.975T$	$0.875T$	$0.75T$	$0.625T$	$0.5T$
Medium	0.86	0.90	0.97	1.00	1.00	0.99
Sum	0.61	0.61	0.67	0.78	0.94	1.00
Min	0.49	0.49	0.49	0.49	0.49	0.49
Max	0.51	0.50	0.50	0.50	0.53	0.86

(c) CelebA (15k)

f	T	$0.975T$	$0.875T$	$0.75T$	$0.625T$	$0.5T$
Medium	0.73	0.76	0.87	0.95	0.97	0.98
Sum	0.53	0.54	0.58	0.68	0.82	0.94
Min	0.50	0.50	0.50	0.50	0.50	0.53
Max	0.49	0.48	0.51	0.50	0.52	0.73

(d) CelebA (20k)

f	T	$0.975T$	$0.875T$	$0.75T$	$0.625T$	$0.5T$
Medium	0.65	0.68	0.78	0.87	0.91	0.93
Sum	0.52	0.52	0.55	0.62	0.73	0.86
Min	0.50	0.49	0.50	0.50	0.50	0.50
Max	0.49	0.49	0.49	0.49	0.50	0.65

Table 11: The **gray-box** attacks AUCROC with different statistic function f and truncation steps T_{trun} (shown in each column) on CelebA across various training set sizes (shown in the title of each sub-table). The first column T corresponds to "no truncation".

We provide additional quantitative results for our gray-box

attack investigating the selection of truncation steps across various training set sizes on CelebA. The results are presented in Table 11, which is supplementary to Figure 8 in the main paper.